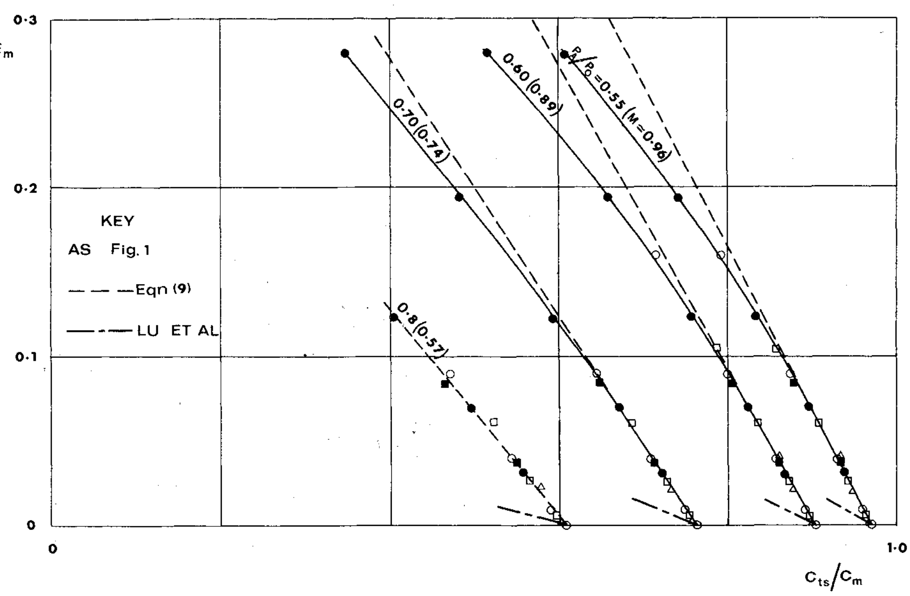

Fig. 2 Variation of static specific-thrust coefficient with swirl intensity, $\gamma = 1.4$.

Table 1 A comparison of calculated values and experimental data

		C_m/C_{m0}		$(C_t/C_m)/(C_t/C_m)_0$	
p_A/p_0	α_{ex}, deg	Theory	Experiment	Theory	Experiment
0.571	23	0.98	0.99	0.98	0.98
0.556	40	0.93	0.92	0.95	0.97

produced by the swirling jet by using the approximate theory previously mentioned. In Fig. 2 curves are plotted which represent the predictions of Lu et al. for the case of outer-biased swirling flow with $\zeta_c^* = 0.8$. These curves are calculated from the appropriate curve in Fig. 17 of Ref. 3. It can be seen from Fig. 2 that the approximate method of Lu et al. leads to substantially larger reductions in specific thrust as compared to the present theory. As a specific example, consider a flow with $p_A/p_0 = 0.55$ and a swirl angle $\alpha_{ex} \equiv \arctan(V_{ex}/W_{ex}) = 25$ deg. The present theory predicts a reduction of 1% in specific static thrust compared to the no-swirl case. The comparable figure according to Lu et al. is approximately 3.5%. This is a significant difference when considering swirl as a possible noise-suppression technique.

In Table 1 the present numerical results are also compared with some of Whitfield's experimental results for outer-biased swirling flows with $\zeta_c^* = 0.6$. In the case of the higher swirl angle some allowance has been made for the fact that the swirl-angle distribution is given at 0.5 diameters downstream of nozzle exit. It can be seen that there is reasonable agreement between the theoretical and experimental values.

In practice, it would be more natural to specify the swirl distribution immediately downstream of the swirler vanes rather than at the nozzle exit. However, upstream axial and swirl velocity profiles corresponding to particular exit conditions can be determined by following the method described in Ref. 6. Also, by following the method described in Ref. 7, the analysis can be easily extended to swirling flows with nonuniform stagnation enthalpy and/or entropy distributions, e.g., swirling flows produced by rotating blades.

References

[1] Schwartz, I. R., "Jet Noise Suppression by Swirling the Jet Flow," AIAA Paper 73-1003, 1973.

[2] Schwartz, I. R., "Minimization of Jet and Core Noise of a Turbojet Engine by Swirling the Exhaust Flow," AIAA Paper 75-503, 1975.

[3] Lu, H. Y., Ramsay, J. W., and Miller, D. L., "Noise of Swirling Exhaust Jets," *AIAA Journal*, Vol. 15, May 1977, pp. 642-646.

[4] Whitfield, O. J., "Novel Schemes for Jet Noise Control," Ph.D. Thesis, Engineering Dept., Cambridge University, 1975.

[5] Bussi, G., "Analisi Numerica di Flussi Vorticosi in Ugelli," Instituto di Macchine e Motori per Aeromobili, Torino, Pub. No. 166, 1974.

[6] Carpenter, P. W. and Johannesen, N. H., "An Extension of One-Dimensional Theory to Inviscid Swirling Flow Through Choked Nozzles," *Aeronautical Quarterly*, Vol. 26, May 1975, pp. 71-87.

[7] Carpenter, P. W., "A General One-Dimensional Theory of Compressible Inviscid Swirling Flows in Nozzles," *Aeronautical Quarterly*, Vol. 27, Aug. 1976, pp. 201-216.

J80-108

Free-Molecule Normal-Momentum Transfer at Satellite Surfaces

20013

Eldon L. Knuth*

University of California, Los Angeles, Calif.

FORCES due to free-molecule normal-momentum transfer at satellite surfaces are of great interest not only because those arising from collisions with atmospheric particles contribute to drag but also because those arising from asymmetric jet impingements introduce additional needs for attitude control. Hence a satellite designer would like to be able to predict these forces for a wide variety of particle species, surface materials, surface roughnesses, and surface contaminants, and for a wide range of particle energies, surface temperatures, and surface coverages.

Received July 10, 1979; revision received Oct. 22, 1979.

Index category: Rarefied Flows.

*Professor of Engineering and Applied Science, Chemical, Nuclear and Thermal Engineering Dept. Consultant, Defense and Space Systems Group, TRW Inc., Redondo Beach, Calif. Associate Fellow AIAA.

A literature search reveals that a modest number of measurements of normal-momentum transfer at technical surfaces (polycrystalline and/or contaminated surfaces) have been reported. Knechtel and Pitts[1] impinged monoenergetic Argon-ion beams, with energy from 15 to 50 eV, on background-contaminated vapor-deposited gold surfaces or thin rolled aluminum sheets. Normal-momentum accommodations were measured for incidence angles θ_i (measured from the surface normal) up to 60 deg; the ion beam was characterized by substituting an ion probe for the target. Doughty and Schaetzle[2] used air, nitrogen, and argon beams with energies from 4 to 200 eV impinging on background-contaminated aluminum (7 rms surface finish) and fresh varnish. Normal-momentum accommodations were measured for θ_i up to 60 deg; the beam was calibrated by substituting a small, hollow, aluminum-foil sphere, with a single opening, for the target. Moskal[3] used a binary-mixture argon-helium supersonic molecular beam with argon energies from 0.06 to 0.53 eV impinging on (100) tungsten surfaces, some of which were uncleaned. Normal-momentum accommodations were measured for the uncleaned surfaces for $\theta_i = 0$ and 33 deg; the beam was calibrated using a stagnation chamber and mass spectrometer to measure the flux and a metastable time-of-flight technique to measure the speed.

Table 1 Normal-momentum accommodation coefficient α_{NM} and normal-momentum flux ratio α'_{NM} as functions of incidence angle θ_i

Symbol	Ref.	Surface	T_wK	Gas	θ_i	α_{NM}	α'_{NM}
○	1	Vapor-deposited gold; $p_b = 2 \times 10^{-5}$ Torr	300-435	Ar^+ at 15 eV	0	1.07	1.11
					10	1.06	1.10
					20	1.06	1.10
					30	1.06	1.10
					40	1.18	1.24
					50	1.42	1.50
					60	1.48	1.59
△	1	Al sheet; $p_b = 2 \times 10^{-5}$ Torr	300-435	Ar^+ at 15 eV	0	1.18	1.22
					10	1.16	1.20
					20	1.15	1.19
					30	1.17	1.22
					40	1.33	1.39
					50	1.55	1.64
					60	1.62	1.74
□	2	Fresh varnish; $p_b = 7 \times 10^{-5}$ Torr	300	N_2 at 25 eV	0	1.07	1.10
					15	1.20	1.24
					30	1.32	1.36
					45	1.47	1.53
					60	1.70	1.80
◇	2	Fresh varnish; $p_b = 7 \times 10^{-5}$ Torr	300	Ar at 25 eV	0	1.03	1.06
					15	1.18	1.22
					30	1.33	1.37
					45	1.44	1.50
					60	1.55	1.64
▽	2	Al; $p_b = 7 \times 10^{-5}$ Torr	300	N_2 at 25 eV	0	1.11	1.14
					15	1.11	1.14
					30	1.15	1.19
					45	1.19	1.24
					60	1.40	1.48
◁	2	Al; $p_b = 7 \times 10^{-5}$ Torr	300	Ar at 25 eV	0	1.07	1.10
					15	1.11	1.14
					30	1.24	1.28
					45	1.32	1.37
					60	1.44	1.52
▼	3	Uncleaned W (100); $p_b = 7 \times 10^{-9}$ Torr	300	Ar at 0.06 eV	0	0.94	1.48
					33	0.89	1.49
◆	3	Uncleaned W (100); $p_b = 7 \times 10^{-9}$ Torr	300	Ar at 0.53 eV	0	1.05	1.27
					33	1.00	1.25
●	4	Mech.-polished sapphire; $p_b = 2 \times 10^{-6}$ Torr	300	He at 0.05 eV	0	0.81	1.26
					10	0.80	1.26
					20	0.80	1.27
					30	0.79	1.30
					40	0.80	1.38
					50	0.79	1.48
					60	0.77	1.62
					70	0.70	1.83
▲	4	Uncleaned Au (111); $p_b = 2 \times 10^{-6}$ Torr	300	He at 0.05 eV	0	0.99	1.54
					10	0.96	1.50
					20	0.94	1.49
					30	0.92	1.51
					40	0.91	1.57
					50	0.90	1.68
					60	0.88	1.86
					70	0.85	2.24
■	5	6061-T6 Al; $p_b = 2 \times 10^{-8}$ Torr	300	He at 1 eV	0	1.29	1.47
					15	1.32	1.51
					30	1.35	1.57
					45	1.42	1.70
					60	1.40	1.80
					75	1.69	2.62

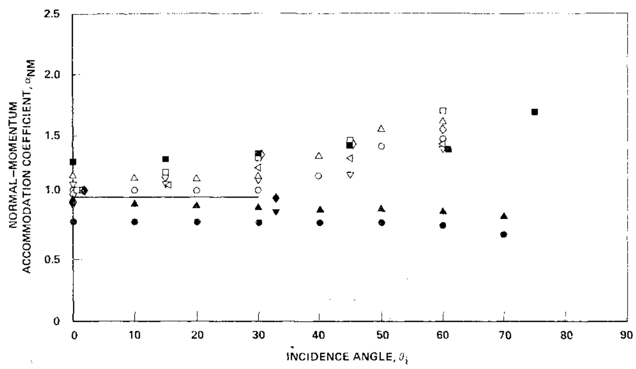

Fig. 1 Normal-momentum accommodation coefficient α_{NM} as function of incidence angle θ_i for the several gas-surface conditions listed in Table 1.

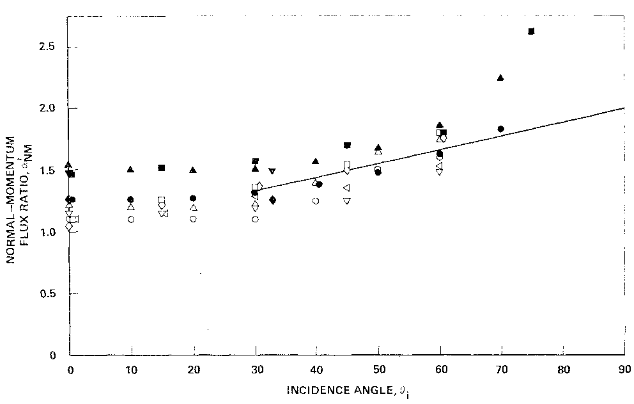

Fig. 2 Normal-momentum flux ratio α'_{NM} as function of incidence angle θ_i for the several gas-surface conditions listed in Table 1.

Seidl and Steinheil[4] impinged a 0.05 eV supersonic helium beam on several different surfaces including a mechanically polished sapphire surface and an uncleaned (111) surface of gold. Normal momentum transfers were measured for θ_i up to 70 deg, the beam was calibrated by substituting a hollow body with a rough internal surface for the target. Liu et al.[5] used a 1-eV arc-heated helium supersonic molecular beam (characterized using a multiple-disk speed filter) impinging on either a 6061-T6 or an anodized 1235-0 aluminum surface. Scattered-beam density and velocity distributions were measured for θ_i up to 75 deg, normal-momentum accommodation coefficients were calculated from these measured distributions by appropriate integrations. The relatively direct procedure for calibration of the incident beam in each of these five studies yields a relatively high level of confidence in the values of the normal-momentum transfers measured in these studies.

A first inclination in an effort to correlate these several data might be to try to adapt the traditional normal-momentum accommodation coefficient[6]

$$\sigma' = \frac{p_{in} - p_{ir}}{p_{in} - p_w} \tag{1}$$

where p_{in} is the normal component of the incident momentum, p_{ir} the normal component of the reflected momentum, and p_w the reflected momentum for complete accommodation, all three of these quantities being positive. However, this coefficient is unsatisfactory for applications in which p_{in} is approximately equal to p_w, i.e., for values of θ_i such that

$$\cos\theta_i \approx \frac{(\pi k T_w / 2m)^{1/2}}{V_i} \tag{2}$$

where k is Boltzmann's constant, T_w the wall temperature, m the particle mass, and V_i the incident speed.

In order to avoid this singularity, Liu et al.[5] used vector quantities,

$$\alpha_{NM} = \frac{p_{in} - p_{ir}}{p_{in} - p_w} = \frac{p_{in} + p_{ir}}{p_{in} + p_w} \tag{3}$$

The results of an effort to correlate the normal-momentum data for engineering surfaces from Refs. 1-5 using α_{NM} are shown in Fig. 1. (See Table 1 for key.) It is seen that α_{NM} handles most of the differences in gas-surface conditions for $\theta_i \leq 30$ deg. More specifically, for $\theta_i < 30$ deg, 80% of the values of α_{NM} fall within 20% of unity. For $\theta_i > 30$ deg, however, relatively large systematic differences are noted; values of α_{NM} for measurements with large values of p_w/p_i are significantly smaller than values of α_{NM} for measurements with smaller values of p_w/p_i. (For the open symbols of Figs. 1 and 2, p_w/p_i ranges from 0.03 to 0.04; for the closed circles and triangles, p_w/p_i equals approximately 0.6; for the remaining symbols, p_w/p_i has intermediate values.) The momentum p_w appearing in the denominator of Eq. (3) appears to exaggerate (for $\theta_i > 30$ deg) the effects of a nonzero surface temperature.

This observation motivates omitting p_w in Eq. (3) and writing

$$\alpha'_{NM} = \frac{p_{in} - p_{ir}}{p_{in}} = \frac{p_{in} + p_{ir}}{p_{in}} \tag{4}$$

Hence the data of Fig. 1 are replotted in Fig. 2 using α'_{NM}. It is seen that α'_{NM} handles most of the differences in gas-surface conditions for $\theta_i \geq 30$ deg. More specifically for $\theta_i \geq 30$ deg, all values of α'_{NM} excepting two fall within 20% of the straight line

$$\alpha'_{NM} = 1 + \theta_i / 90 \text{ deg} \tag{5}$$

(The two exceptions are for relatively large incidence angles, where measurements are more difficult.) The limiting value, $\alpha'_{NM} = 2$, is of physical interest since it is consistent with an elastic reversal of p_{in}, i.e., with $p_{ir} = p_{in}$.

Note, for $\theta_i > 30$ deg, the insensitivity of α'_{NM} to gas-surface conditions. The conditions represented in Fig. 2 include both monatomic and diatomic incident-particle species; surfaces as different as those for single-crystal gold, relatively fresh varnish, and aluminum sheet; and incident-particle energies from 0.05 to 25 eV.

In view of the need to predict forces due to free-molecule normal-momentum transfers at satellite surfaces, including transfers at large incidence angles, additional laboratory and/or satellite measurements on technical surfaces are strongly recommended. Since almost no data are available for $\theta_i > 60$ deg, and since the available data indicate only modest influences of particle species, surface materials, surface roughness, surface contaminant, particle energy, and surface coverage (at least for ranges typical of satellite applications), it is recommended further that special attention be given to measurements with $\theta_i > 60$ deg. In the interim, for satellite designs when specific information for the given gas-surface combination is lacking, it is suggested that $\alpha_{NM} = 1$ be used for $\theta_i \leq 30$ deg (see Fig. 1) and that $\alpha'_{NM} = 1 + \theta_i / 90$ deg be used for $\theta_i > 30$ deg (see Fig. 2). The definitions of the coefficients α_{NM} [Eq. (3)] and α'_{NM} [Eq. (4)] deviate significantly from the definition of the traditional normal-momentum accommodation coefficient σ' [Eq. (1)]. However, all three definitions are arbitrary, and α_{NM} and α'_{NM} have the advantages of 1) no singularity at $p_i \cos\theta_i = p_w$ and 2) a demonstrated usefulness in correlations of data over relatively wide ranges of θ_i.

Acknowledgments

This work was performed under a TDRSS contract from Western Union to TRW. The author appreciates the contributions to this Note of stimulating discussions with J.T. Ohrenberger and C.N. Tsu of TRW Inc.

References

[1] Knechtel, E.E. and Pitts, W.C., "Experimental Momentum Accommodation on Metal Surfaces of Ions Near and Above Earth-Satellite Speed," *Rarefied Gas Dynamics*, edited by L. Trilling and H.Y. Wachman, Vol. 2, Academic Press, New York, 1969, pp. 1257-1266.

[2] Doughty, R.O. and Schaetzle, W.J., "Experimental Determination of Momentum Accommodation Coefficients at Velocities up to and Exceeding Earth Escape Velocity," *Rarefied Gas Dynamics*, edited by L. Trilling and H.Y. Wachman, Vol. 2, Academic Press, New York, 1969, pp. 1035-1054.

[3] Moskal, E.J., "An Investigation of the Normal Momentum Transfer for Gases on Tungsten," Univ. of Toronto Institute for Aerospace Studies, Toronto, UTIAS Rept. 166, June 1971.

[4] Seidl, M. and Steinheil, E., "Measurement of Momentum Accommodation Coefficients on Surfaces Characterized by Auger Spectroscopy, SIMS, and LEED," *Rarefied Gas Dynamics*, edited by M. Becker and M. Fiebig, Vol. II, DFVLR-Press, Porz-Wahn, Germany, 1974, Paper E. 9.

[5] Liu, S.-M., Sharma, P.K., and Knuth, E.L., "Satellite Drag Coefficients Calculated from Measured Spatial and Energy Distributions of Reflected Helium Atoms," *AIAA Journal*, Vol. 17, Dec. 1979, pp. 1314-1319.

[6] Schaaf, S.A. and Chambré, P.L., "Flow of Rarefied Gases," *Fundamentals of Gas Dynamics* edited by H.W. Emmons, Princeton Univ. Press, Princeton, 1958, pp. 687-739.

J80-109

Recent Experiments on Heterogeneous Detonation Waves

20008
20015

J. A. Nicholls,* R. Bar-Or,† Z. Gabrijel,‡
and
E. Petkus§
The University of Michigan, Ann Arbor, Mich.

Introduction

THIS Note presents some recent results of an ongoing study of the blast wave initiation and propagation of cylindrical heterogeneous detonation waves. Particular aspects of interest in this study are the details of and the initiator energy required for the initiation of detonation, the characteristics of the wave propagation, the influence of physical and chemical properties of the fuel, and wave propagation through a cloud which is nonuniform in fuel-oxidizer ratio.

The experimental facility employed is essentially the same as that described earlier[1,2] so that only a cursory description will be given here. The sectored shock tube, shown in Fig. 1, is designed to model a sector of a cylindrical combustible cloud. The angle of the sector is 20 deg, the "height" of the cloud (distance between the side walls) is 5.2 cm, and the radius is about 140 cm. The fuel drops are dispersed throughout the gaseous oxidizer by flowing the liquid fuel through as many as 322 needles and pulsing this flow at about the Rayleigh frequency. With the current size of needles in use, the resultant uniform drop size is about 400 μm. The cylindrical blast wave is formed by firing a blasting cap (Dupont E-106) and a measured amount of condensed explosive (Dupont Detasheet C). The propagation of the wave in the radial direction is monitored by 14 time-of-arrival pressure switches. This position-time data can then be converted to velocity vs radius information.

The chamber was operated with 42 rows with seven needles (0.02 cm i.d.) per row. For the oxygen case, the fuel flow was maintained constant and the air replaced by oxygen. As a consequence, the mixture ratio was quite lean in the oxygen studies. The theoretical Chapman-Jouguet detonation velocities, as calculated by the Gordon-McBride program[3] where the fuels were assumed to be in the gaseous phase but the enthalpy of formation used was that of the liquid, were 1810 and 1876 m/s for kerosene in air and oxygen, respectively, or 1850 and 1812 m/s for 75/25 kerosene + NPN in air and oxygen, respectively.

Experimental Results

A series of experiments was conducted whereby strong blast waves, generated by various amounts of condensed explosives, propagated into sprays of kerosene droplets in air and in oxygen. In the case of sprays in air, detonation waves were not attained and the blast waves in the sprays attenuated even faster than blast waves in air alone (no droplets). In the case of sprays in oxygen, detonations were attained even for the lowest initiation energy used.

Figure 2 represents results for various run conditions for a constant initiation energy level. As can be seen, the blast wave in air (no fuel) is somewhat faster than the reacting blast wave (no detonation) in kerosene and air, which, in turn, is only slightly faster than a blast wave propagating in kerosene spray in nitrogen (not shown on Fig. 2). These results indicate the attenuating effect of the droplets on the blast wave. The blast wave in a spray of kerosene in oxygen decays to a constant velocity of 1600 m/s, indicating that detonation has been attained but at a lower velocity than theoretical (1876 m/s).

Some further experimental results in kerosene-oxygen for different energy levels are shown in Fig. 3. It can be noted that the higher energy levels produce stronger blast waves which

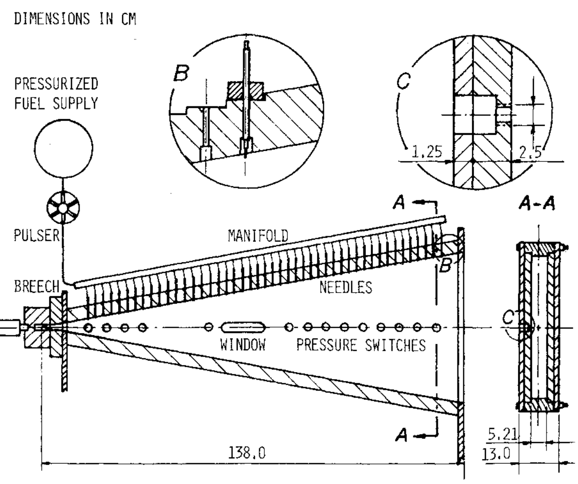

Fig. 1 Schematic of detonation chamber.

Presented as Paper 79-0288 at the AIAA 17th Aerospace Sciences Meeting, New Orleans, La., Jan. 15-17, 1979; submitted Feb. 27, 1979; revision received Oct. 17, 1979.

Index categories: Shock Waves and Detonations; Multiphase Flows.

*Professor, Aerospace Engineering Dept. Associate Fellow AIAA.
†Doctoral Candidate, Aerospace Engineering.
‡Doctorate completed; now in Yugoslavia.
§Student, Aerospace Engineering. Student Member AIAA.